To appear in ApJ

Mid-infrared Spitzer spectra of X-ray selected Type 2 QSOs: QSO2s are not ULIRGs

E. Sturm, G. Hasinger, I. Lehmann, V. Mainieri, R. Genzel, M.D. Lehnert, D. Lutz, and L.J. Tacconi

Max-Planck-Institut für extraterrestrische Physik, Postfach 1312, D-85741 Garching, Germany

sturm@mpe.mpg.de

ABSTRACT

We have performed a spectroscopic study of 7 Type 2 QSOs using the mid-infrared spectrometer *IRS* on board the *Spitzer Space Telescope*. These are (to our knowledge) the first mid-IR spectra of X-ray selected QSO2s taken. The objects have been selected according to their high intrinsic luminosities and column densities in the X-rays. Their spectra strongly differ from template spectra of Type 2 AGN at lower luminosities. They do not exhibit strong PAH dust emission features from circum-nuclear star forming regions, typical for lower luminosity Type 2 Seyfert galaxies or other previously used QSO2 templates, such as the (Ultra)luminous Infrared Galaxy ((U)LIRG) NGC 6240. They also do not show the ice and silicate absorption features of highly luminous but deeply embedded compact nuclei seen in some ULIRGs. Instead they reveal a relatively featureless, rising continuum similar to luminous Type 1 AGN. We also find evidence for a 10μm silicate feature in *emission*. Models of dusty tori in the AGN unification scenario predict this only for Type 1 AGN. The ratio of the AGN continuum luminosity at 6μm to the absorption corrected 2-10keV X-ray AGN luminosity is very similar to that found in Seyfert galaxies. X-ray selected QSO2s are thus characterized by powerful AGN in hosts with a luminosity due to star formation $\lesssim 10^{11}$L$_\odot$. The dominance of the AGN light in the mid-IR spectra of QSO2s together with their flatter spectral energy distributions (SEDs) places important constraints on models of the cosmic infrared background and of the star formation history of the universe.

Subject headings: galaxies: quasars — galaxies: active — galaxies: evolution

1. Introduction

Intrinsically luminous, but highly obscured active galactic nuclei (AGN), the Type 2 QSOs (QSO2s), have long been sought as a crucial (and necessary) component of AGN unification theories and of models that explain the cosmic X-ray and infrared background by the growth of obscured supermassive black holes throughout cosmic history. In unified models different types of AGN are postulated to all harbor a central, accreting massive black hole surrounded by a Broad Line Region (BLR). The AGN is proposed to be surrounded by dusty obscuring material, often modeled as a (clumpy) torus, that anisotropically absorbs or shadows emission from the nuclear region. Further out a system of gas (and dust) clouds, the Narrow Line Region (NLR), emits highly excited narrow lines that are ionized by the central source. Broad-line, Type 1 AGN in this scheme are AGN where the line of sight to the nucleus is not blocked. In narrow-line, Type 2 systems the line of sight to the nucleus is blocked by the obscuring torus, and only the narrow line region is directly visible. Besides orientation, the luminosity/activity level is the second primary physical parameter differentiating AGN, from Low Luminosity AGN to Seyferts to QSOs.

Population synthesis models of the cosmic X-ray background (XRB) try to explain the hard spectrum of the XRB by a mixture of absorbed and unabsorbed AGN, spread over a large redshift interval (e.g. Setti & Woltjer 1989), folded with the corresponding luminosity function and its cosmological evolution. Such models were developed within the unified AGN scenario, often assuming a fraction of obscured (Type 2) to unobscured (Type 1) objects as in local AGN (ascribed to the covering factor of the torus which is assumed to be the same for all luminosites). They require that a significant fraction of the cosmic black hole growth is obscured by large amounts of dust and gas. Hence, a substantial contribution to the XRB should come from intrinsically luminous, obscured X-ray sources, i.e. QSO2s.

In the Seyfert domain unification theories are very successful. The existence of obscured QSOs, however, as the high-luminosity analogues of the Seyfert 2 galaxies, has been hotly debated since the formulation of the first unified theories. Radio-loud QSO2s, i.e. radio galaxies, have been the only observed Type 2 QSOs for a long time. However, radio galaxies represent only a small fraction of the total AGN population. Radio quiet QSO2s remained elusive until very sensitive and deep hard x-ray imaging and spectroscopy campaigns became feasible with the advent of Chandra and XMM-Newton (Dawson et al. 2001, Norman et al. 2002, Mainieri et al. 2002, Stern et al. 2002, Hasinger et al. 2003, Della Ceca et al. 2003). In the X-ray domain the QSO-2 population is characterized by high intrinsic absorption ($N_H > 10^{22}$ cm^{-2}), and high intrinsic X-ray luminosity (L[0.5-10keV] $> 10^{44}$ erg/s).

According to both AGN unification and XRB models, QSO2s should be more numerous than Type 1 QSOs. From XMM-Newton observations of the Lockman Hole we (Mainieri

et al. 2002) found indeed a large fraction of the objects to be obscured AGN. However, the number of identified *luminous* sources, i.e. QSO2s, amongst them is very low compared to the model assumptions. The fraction of Type 2 objects in these surveys decreases with increasing X-ray luminosity (Ueda et al. 2003, Hasinger 2003). A similar trend has been found in optical studies based on QSOs from the SDSS (Simpson 2005). This trend might indicate a breakdown of those unification models where the covering factor is independent of luminosity. An alternative explanation might be that many QSO2s are so obscured that they are hidden even at hard X-rays ('Compton thick', $N_H > 10^{24}$ cm^{-2}). Recently, deep mid-infrared imaging studies with Spitzer, using mid-IR/radio color criteria, have begun to detect a population of Type 2 QSOs which seem to be at least comparable in number density to the un-obscured Type 1 population (Martinez-Sansigre et al. 2005, Donley et al. 2005). Some of these objects show no hard X-ray counterpart, indicating that these QSOs are hidden by Compton thick material even at high X-ray energies.

In this paper we present the first mid-infrared spectra of QSO2s. The objects have been selected according to their X-ray luminosity and column density (section 2). The spectra and the multi-wavelength spectral energy distributions (SEDs) of our QSO2s allow us to discuss the mid-infrared properties of such QSO2s by comparing them to various template spectra of active galaxies (section 3). We study the relative contributions from star formation and obscured AGN to their total energy output (section 4), and we investigate the putative luminosity dependence of the relative abundance of Type 2 vs. Type 1 objects (section 5).

2. Sample Selection, Observations, Data Processing

We have selected the QSO2s for this program from our deep ($\approx$ 1Msec) XMM-Newton observations of the Lockman Hole (Hasinger et al. 2001, Mainieri et al. 2002). We picked those objects with high intrinsic absorption (with a mean $N_H \approx 1.0\text{x}10^{23}$ cm^{-2}, as derived from absorbed power law fits), and high intrinsic (absorption corrected) X-ray luminosities (L[0.5-10keV] $> 10^{44}$ erg/s). From this list of objects we culled the ones which, in addition, have ISOCAM detections with a flux density at 15 μm of greater than 0.3 mJy (Fadda et al. 2002). As a control target in order to examine the role of luminosity in this selection method we have also selected one source (LH901A) with similarly high X-ray absorption, but slightly lower intrinsic luminosity. Furthermore, we have performed optical spectroscopy on our targets, which yielded narrow emission lines typical of Type 2 AGN without associated broad components (Lehmann et al. 2000, 2001).

We have augmented the sample by 3 targets with similar information from the literature: the QSO2 'proto-type' CDF-S 202 (CXOCDFS J033229.9-275106) from the Chandra Deep

Field-South (Norman et al. 2002), CXO 52 (CXO J084837.9+445352, Stern et al. 2002), and AX J0843+2942 (della Ceca et al. 2003). The latter source is a radio loud QSO2 candidate, which we chose to investigate the radio loud end of the QSO2 phenomenon. These 8 sources also cover a large redshift range from 0.2 to 3.7. The targets are listed in Table 1.

Our data were obtained with the Spitzer IRS (Houck et al. 2004; Werner et al. 2004) as a GO Cycle-1 project (PI: E. Sturm, PID 3223). Because of the relative faintness of our objects they were observed in low resolution mode only, restricted to the one or two IRS slits and orders, which (together) covered a rest wavelength range of approximately 5 to 12μm. Exposure times were typically between 4800 and 8400 seconds in the LL module (20 to 35 nod1-nod2 cycles of 120s at each nod position), and between 3840 and 7200 seconds in the SL module (8 to 15 cycles of 240s per nod).

Our data reduction started with the two-dimensional BCD products from the Spitzer pipeline (S12). We removed the sky background by a pairwise subtraction of frames at different nod positions for each cycle. Using the pipeline bad pixel mask (bmask) and sigma clipping algorithms we removed (de-glitch) bad or noisy pixels, replacing them by an interpolation of the neighboring pixels. The resulting nod1-nod2 frames were then co-added by averaging, resulting in a single, filtered, frame with a positive and a negative beam. We used the software package SMART (Higdon et al. 2004) to extract calibrated one dimensional spectra for the positive and negative beams (using the 'interactive/column/No SkySub' method). These were then averaged into the final spectra.

In the case of LH H57 a second object appears in the LL2 slit, which partially overlaps with LH H57. This second object is located approximately 10″(2 pixels) SE of LH H57 (PA≈125° E of N). It is therefore not visible in the SL1 slit, which has a smaller slit width and a different orientation. We have extracted the LL2 spectra of both objects by using the 'fixed column' method in SMART. This has caused some flux loss (and increased flux calibration uncertainty) for either of the two spectra, but allowed a qualitative separation of the two objects. The second object appears to be starburst dominated, and we tentatively assign a redshift of z ≈ 0.58 for that second source, by identifying the two major peaks in the spectrum with the 11.3 and 12.7 μm PAH features.

3. Mid-infrared spectral properties and global SEDs

The spectra are shown in Fig. 1 and Fig. 2. With the exception of CXO 52 Lynx all objects were detected. We derive an upper limit for CXO 52 in the 5 - 9 μm rest (20 - 40 μm observed) wavelength range of 0.1 mJy. All the spectra show a rising mid-infrared

continuum, typical of AGN. There are no strong hints of absorption from silicates (9.6 μm), ices (6 μm) or hydrocarbons (6.8 μm), which would be typical of highly obscured objects. Dust emission features (PAHs) from star forming regions are very weak or absent, with the obvious exception of LH 901A (Fig. 2), the object with the lowest intrinsic X-ray luminosity of our sample. No strong ionic or molecular (narrow) emission lines can be seen in these faint, low resolution spectra. Only LH 901A and LH 28B show weak lines of [S IV], [Ar III] and H_2. We have computed an average spectrum (scaled with the 6μm flux) using LH 12A, 14Z, 28B, H57, and AXJ0843, which is shown in Fig. 3. In this average spectrum we identify (unresolved) narrow emission lines of [Ar II]6.9μm (probably blended with H_2 S(5)), [Ar III]9.0μm (potentially blended with [Mg VII]), [Ne VI]7.6μm, and H_2 S(3)9.6μm. For comparison we show in Fig. 3 the IRS spectrum of a luminous Type 1 AGN, the QSO PG1426+015, a typical PG QSO from a large study (QUEST) of ULIRGs and PG QSOs (Veilleux et al., in preparation). This comparison supports the conclusion that the spectra of our objects exhibit continuous spectra like luminous Type 1 AGN in the mid-infrared regime, despite being selected as highly obscured, Type 2 AGN in the X-rays.

This absence of PAH and/or absorption features is remarkable and surprising. QSO2s are often believed to be related to Ultraluminous Infrared Galaxies (ULIRGs). ULIRGs are extremely dusty, highly obscured galaxies with space densities and luminosities comparable to local QSOs (Sanders & Mirabel 1996). In particular NGC 6240, a nearby infrared luminous system, is frequently used as type 2 AGN template (e.g. Lehmann et al. 2002, Norman et al. 2002) because its X-ray and mid-infrared properties identify it as hosting a highly obscured AGN (Lutz et al. 2003, and references therein). The mid-IR spectrum of NGC 6240, however, exhibits strong dust emission features quite different from our QSO2 spectra (but very similar to LH901A, see the comparison in Fig. 2). Some local ULIRGs, like IRAS F00183-7111 (Tran et al. 2001, Spoon et al. 2004), and many mid-infrared sources at higher redshifts (Houck et al. 2005, Yan et al. 2005), are dominated by absorbed continua, shaped by deep absorption features of silicates, ices, and hydrocarbons, indicating compact, deeply embedded nuclei that could plausibly be AGN. These sources are alternative template candidates for QSO2s. However, the objects presented here clearly do not resemble these dust absorbed ULIRGs.

Even more remarkable, the average QSO2 spectrum appears to exhibit a 10μm silicate feature in *emission*, even if our spectra do not extend far enough beyond 10μm to cover the full emission feature. The PG QSO shown in Fig. 3 covers a broader range and exhibits a clear 10μm silicate emission feature. From the close similarity of the two spectra we conclude that the average QSO2 spectrum shows a comparable emission feature. Silicate emission was recently found in many PG QSOs (Siebenmorgen et al. 2005, Hao et al. 2005, Sturm et al. 2005). Many AGN torus models predict such a silicate emission as a signature of the obscuring torus. According to unification models silicates should appear

in emission in Type 1 AGN, but in absorption in Type 2 AGN. Sturm et al. (2005) have urged caution that this may not be the full explanation for the observed silicate emission in QSOs, and that at least some emission may arise in more extended regions, like a dusty narrow line region. They substantiate this claim with the relatively cool (200K) temperature of the silicate dust (as derived from the ratio of the emission features at 10 and 18 μm), which seems too cold to be explained by a hot inner torus wall, but which is consistent with observed color temperatures of extended dust found in the narrow line regions of some nearby Seyfert galaxies. The presence of silicate emission in Type 2 QSOs, if confirmed in future observations, would pose further important constraints on the origin of dust emission in AGN.

We have collected the multi-wavelength (X-ray-to-radio) SEDs of our objects, using our ancillary data and data from the literature (Norman et al. 2002, Stern et al. 2002, della Ceca et al. 2003). In Figure 4 we compare these SEDs to the SEDs of NGC 6240 and an average Seyfert 2 SED, composed from a sample of local galaxies by Schmitt et al. (1997, soft X-ray to radio range) and Moran et al. (2001, hard X-ray range). The average Seyfert 2 spectrum has a lower infrared/X-ray ratio than NGC 6240 (see Figure 4, lower left panel). For most objects we have scaled the comparison SEDs to the X-ray data. For LH14Z, 28B, and H57, which are unusually X-ray bright, we have scaled to the near-IR data. In order to predict a flux density at 100μm, the wavelength around which the SEDs of many galaxies have their peak, we have measured 3σ upper limits for the PAH 7.7μm peak flux densities (above the continuum). This PAH peak height ($S_{7.7}$) is a reasonable tracer of the star formation related far-IR flux of active galaxies (e.g. Lutz et al. 2003). In M 82, a prototypical starburst galaxy (shown in Fig. 2), the ratio of the 7.7μm PAH peak height to the 100μm flux density (S100), both measured in Jy, is 0.069 (derived from the ISOCAM-CVF spectrum, Förster Schreiber et al. 2003, and the ISO-LWS spectrum, Colbert et al. 1999). This ratio is very similar in many starburst galaxies, with a dispersion of about 35% (Rigopoulou et al. 1999). Using this value we predict 100μm flux density limits for the QSO2s. They are listed in Table 1 (denoted as $S100_{PAH}$) and indicated as asterisks in Figure 4. The optical-to-near-IR SEDs of most of our objects are quite similar to the average Seyfert 2 galaxy, or to NGC 6240. At these wavelengths (and within the redshift range of our objects) the emission of Type 2 quasars is probably dominated by starlight from the host galaxy. The mid-to-far infrared SEDs of these QSOs, however, are clearly flatter (have smaller mid-far-IR/near-IR ratios) than normal Type 2 template objects, if our PAH based extrapolation is applicable. Only LH901A, with its intrinsic X-ray luminosity more in the range of normal Seyferts than of QSOs, matches quite nicely the NGC 6240 template. The mid-IR SEDs of QSO2s are therefore on average warmer than for Type 2 template objects of lower luminosity, probably with only a weak (rest-frame) far-IR peak, due to a strong AGN contribution as revealed by

the mid-IR spectra. We estimate the star formation related far-IR (8-1000μm) flux, $F_{IR,SF}$, and luminosity, $L_{IR,SF}$, again from the measured PAH peak flux density limits, applying a ratio of $\log(S_{7.7}/F_{IR,SF}) = 12.0$, as measured in M 82. The corresponding values of $L_{IR,SF}$ for our targets are listed in Table 1. With values (limits) of a few x $10^{10} L_{\odot}$ they lie in a range which is very typical for local starburst galaxies but well below ULIRGs.

Our decision to select only those objects with a (estimated) 15μm flux density above 0.3mJy might have caused some selection effect, favoring AGN-like objects with strong mid-IR continua. We note, however, that the 0.3 mJy level does not impose a severe cut-off, in the sense that at such a flux density we would have detected PAH dominated objects like NGC 6240, too. NGC 6240 itself would be detectable with *IRS* out to a redshift of $\sim$ 1.5. If CXO 52 were NGC 6240-like (but at higher absolute flux level, scaling with the X-ray luminosity) we would have detected it (see Fig. 4).

4. The relative contributions of star formation and AGN

A quantitative estimate of the contribution of obscured AGN to the X-ray and infrared backgrounds is crucial to deduce the star formation history of the universe from galaxy luminosity functions (see section 1), and it is important to understand the evolution of galaxies and AGN. In contrast to their lower luminosity AGN cousins, the Seyfert 2 galaxies, contributions of the host galaxies to the mid-IR spectra of QSO2s seem to be small, since typical star-formation tracers such as PAH emission features are mostly absent. In order to quantify this we have performed a decomposition of the spectra into a starburst template (M 82) and an AGN template (linear continuum) in the same way as described in Lutz et al. (2004): in the range covered by our IRS spectra the AGN emission is best isolated shortward of the complex of aromatic emission features (Laurent et al. 2000). We determine a continuum at 6μm rest wavelength, and eliminate non-AGN emission. This is done by subtracting the PAH template scaled with the strength of the aromatic features arising in the host or in circum-nuclear star formation.

The resulting 6μm AGN continua are listed in Table 1. The AGN contribution to the total flux density at 6μm is 67% for the lower luminosity source LH901A, and close to 100% for the QSO2s (except CDF-S202 and CXO 52 where we could not measure it). QSO2s likely represent a significant component of the high redshift AGN population. Since their infrared spectra are more AGN dominated (i.e. flatter) than less luminous Type 2 AGN, their contribution to the peak of the cosmic infrared background is lower than predicted using these less luminous templates. Future models of the star formation history and the cosmic infrared background have to take this into account. The flatter infrared SEDs of these

QSO2s also explain (at least partially) the low success rate of previous attempts to detect these objects in the (sub-)mm with SCUBA and MAMBO (e.g. Chapman et al. 2004), if we assume a similar 100μm/850μm flux density ratio as in the lower luminosity templates.

5. The relation between mid-infrared continuum and hard X-ray emission

Hard X-rays, unless extremely absorbed in Compton-thick objects, can provide a direct view to the central engine. They are, therefore, a measure of the bolometric luminosity of the AGN. The nuclear infrared continuum in AGN, in contrast, is due to a re-processing of the AGN emission by the circum-nuclear dust, e.g. in the putative torus. The observed mid-infrared AGN emission is thus a function of both the AGN luminosity and the distribution of the obscuring matter. As mentioned in the introduction one important result of the hard X-ray studies is the decreasing fraction of Type 2 objects with increasing X-ray luminosity. A possible explanation of this trend may be that high luminosity objects are able to 'clean out' their environment by ionizing the circumnuclear matter and/or producing strong outflows, while low luminosity objects are largely surrounded by the circumnuclear starburst region from which they are being fed. A similar scenario is provided by the 'receding torus' models (e.g. Lawrence 1991, Simpson 2005). In these models the opening angle of the torus (measured from the torus axis to the equatorial plane) is larger in more luminous objects because the distance of the inner torus wall to the nucleus, which is determined by the dust sublimation temperature, increases with luminosity (while the torus height stays constant). If this trend of decreasing Type 2 AGN fraction with increasing luminosity is indeed related to a decreasing covering factor the ratio of mid-IR continuum (re-radiation) and intrinsic X-ray emission should be lower in QSO2s than in Seyfert2s.

Lutz et al. (2004) have examined this ratio of hard X-ray to mid-IR continuum luminosities in a large sample of local Seyfert galaxies (and a few QSO1s), based on the decomposition of their mid-IR spectra into AGN and starburst components as described above. They found a good correlation (with some scatter) and no difference between Type 1 and Type 2 objects. In Table 1 we list the X-ray/mid-IR ratios of our QSO2s, derived in the same way as in Lutz et al. (2004). The ratios are very similar (within the dispersion) to the ratios in Seyfert galaxies, while a decreasing covering factor would cause an increase of the relation at high luminosities. However, given the scatter in our data and the variability of the X-ray data small changes in covering factor would be difficult to detect. Our data are thus consistent with a constant Type 2/Type 1 ratio, but we cannot exclude modest luminosity dependencies of the covering factor at this stage. On the other hand, the observed X-ray/mid-IR correlation offers an explanation for the overall mid-IR spectral properties of QSO2s: the

AGN continuum at mid-IR wavelengths simply scales with the high AGN luminosities in our objects and outshines any contribution from circum-nuclear star forming regions ($\lesssim 10^{11} L_{\odot}$, see section 3). The reason for the constancy of this relation and the similarity of Type 1 and Type 2 AGN in that respect remains an open question. Lutz et al. (2004) have tentatively attributed this similarity to extended dust emission, because significant non-torus contributions to the AGN mid-IR continuum could mask the expected difference between the two types of AGN. Our QSO2 study, which extends this similarity of Type 1 and Type 2 AGN to the quasar regime, and which indicates silicate emission (rather than absorption) in Type 2 QSOs, has added evidence that at least some of the mid-IR dust emission in AGN arises in extended regions.

This work is based on observations made with the Spitzer Space Telescope, which is operated by the Jet Propulsion Laboratory, California Institute of Technology under NASA contract 1407. We are grateful to Hagai Netzer for inspiring discussions.

REFERENCES

Chapman, S. C., Smail, I., Blain, A. W., & Ivison, R. J. 2004, ApJ, 614, 671

Colbert, J. W., et al. 1999, ApJ, 511, 721

Dawson, S., et al. 2001, AJ, 122, 598

Della Ceca, R., et al. 2003, A&A, 406, 555

Donley, J.L., et al. 2005, astro-ph/0507676

Förster Schreiber, N. M., Sauvage, M., Charmandaris, V., Laurent, O., Gallais, P., Mirabel, I. F., & Vigroux, L. 2003, A&A, 399, 833

Hao, L., et al. 2005, ApJ, 625, L75

Hasinger, G., et al. 2001, A&A, 365, L45

Hasinger, G. 2003, astro-ph/0310804

Higdon, S. J. U., et al. 2004, PASP, 116, 975

Houck, J. R., et al. 2004, ApJS, 154, 18

Laurent et al. 2000, A&A, 359, 887

Lawrence, A. 1991, MNRAS, 252, 586

Lehmann, I., Hasinger, G., Schmidt, M., et al. 2000, A&A, 354, 35

Lehmann, I., Hasinger, G., Schmidt, M., et al. 2001, A&A, 371, 833

Lehmann et al. 2002, ASP Conf. Ser. 262, 105

Lutz, D., Sturm, E., Genzel, R., Spoon, H. W. W., Moorwood, A. F. M., Netzer, H., & Sternberg, A. 2003, A&A, 409, 867

Lutz, D., Maiolino2, R., Spoon, H.W.W., and Moorwood, A.F.M. 2004, A&A, 418, 465

Mainieri, V., et al. 2002, A&A, 393, 425

Martinez-Sansigre, A., et al. 2005, Nature, 436, 666

Moran, E.C., et al. 2001, ApJ, 556, L75

Norman, C. et al. 2002, ApJ, 571, 218

Sanders, D. B., & Mirabel, I. F. 1996, ARA&A, 34, 749

Schmitt, H.R., Kinney, A.L., Calzetti, D., and Storchi Bergmann, T. 1997, AJ, 114, 592

Setti, G. & Woltjer, L. 1989, A&A, 224, L21

Siebenmorgen, R., Haas, M., Krügel, E., & Schulz, B. 2005, A&A, 436, L5

Simpson, C. 2005, MNRAS, 360, 565

Spoon, H.W.W., ApJS, 154, 184

Stern, D. et al., 2002, ApJ, 568, 71

Sturm, E., Lutz, D., Tran, Q.D., et al. 2000, A&A,358, 481

Sturm, E., et al. 2005, ApJ, 629, L21

Tran, Q.D. et al. 2001, ApJ, 552, 527

Ueda, Y. et al. 2003,

Werner, M. W., et al. 2004, ApJS, 154, 1

Table 1: The QSO2 sample, X-ray, and infrared properties.

Source	RA	DEC	z	log L_x	log N_H	$S_{AGN,6}$	$L_x/\nu L_{\nu,6}$	$S100_{PAH}$	$L_{FIR,SF}$
	Equatorial J2000					[mJy]		[mJy]	[$10^{10}L_\odot$]
LH 12A	10h51m48.80s	+57d32m48.0s	0.990	44.3	22.7	0.58	0.21	<0.6	<2.5
LH 14Z	10h52m42.20s	+57d31m58.0s	1.38	44.9	22.6	0.20	0.36	<0.6	<4.9
LH 28B	10h52m50.30s	+57d25m44.0s	0.205	44.2	21.3	1.63	1.39	<3.4	<0.5
LH 901A	10h52m52.80s	+57d29m00.0s	0.205	43.1	23.5	0.45	0.32	14.4	2.2
LH H57	10h53m05.70s	+57d28m10.3s	0.792	44.0	22.4	0.20	0.32	<0.8	<1.9
CDF-S 202	03h32m29.86s	-27d51m05.8s	3.700	45.0[1)]	>24	0.18	0.23	-	-
CXO 52 Lynx	08h48m37.90s	+44d53m52.0s	3.288	44.5[1)]	23.7	<0.1	<0.2	-	-
AX J0843+2942	08h43m09.90s	+29d44m04.9s	0.398	45.5	23.2	4.20	2.67	<5.1	<3.0

col(1): target name; col(2): RA; col(3):DEC; col(4):redshift; col(5): intrinsic luminosity L[0.5-10keV] in erg/s; col(6): intrinsic absorption log(N_H) in cm^{-2}, col(7): AGN continuum at 6μm in [mJy], estimated from spectral decomposition; col(8): intrinsic 2-10keV luminosity vs. AGN continuum luminosity ($\nu L_\nu(6\mu m)$; col(9): predicted (upper limit of the) flux density at 100μm in [mJy], derived from 7.7μm PAH strength/limit; col(10): star formation related 8-1000μm luminosity, estimated from 7.7μm PAH

1) 2-10 keV

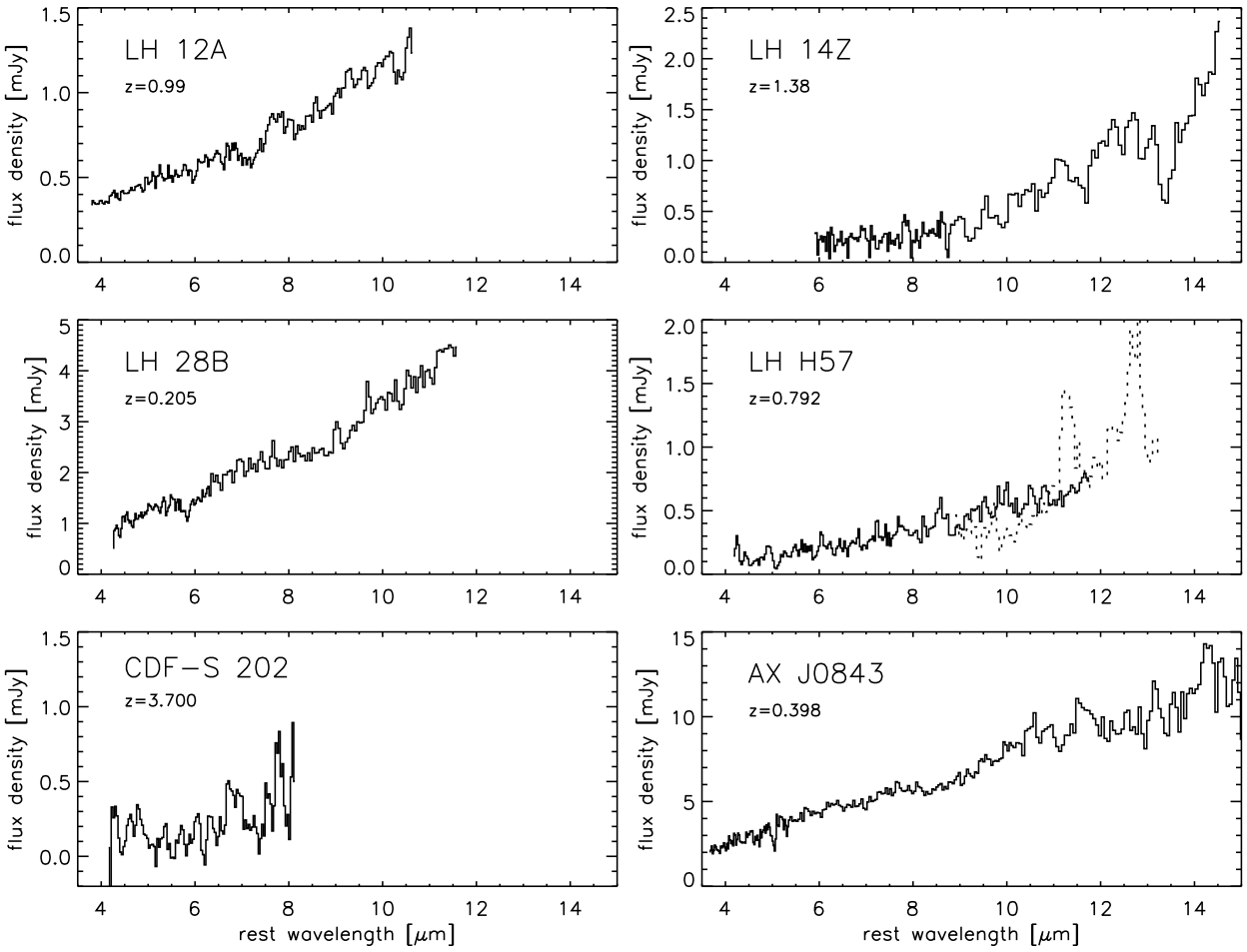

Fig. 1.— IRS spectra of 6 of the 7 QSO2s. CXO 52 Lynx was not detected. The dotted line in the LH H57 panel is the spectrum of the second source in the LL2 slit which is partly blended with LH H57, assuming z=0.579.

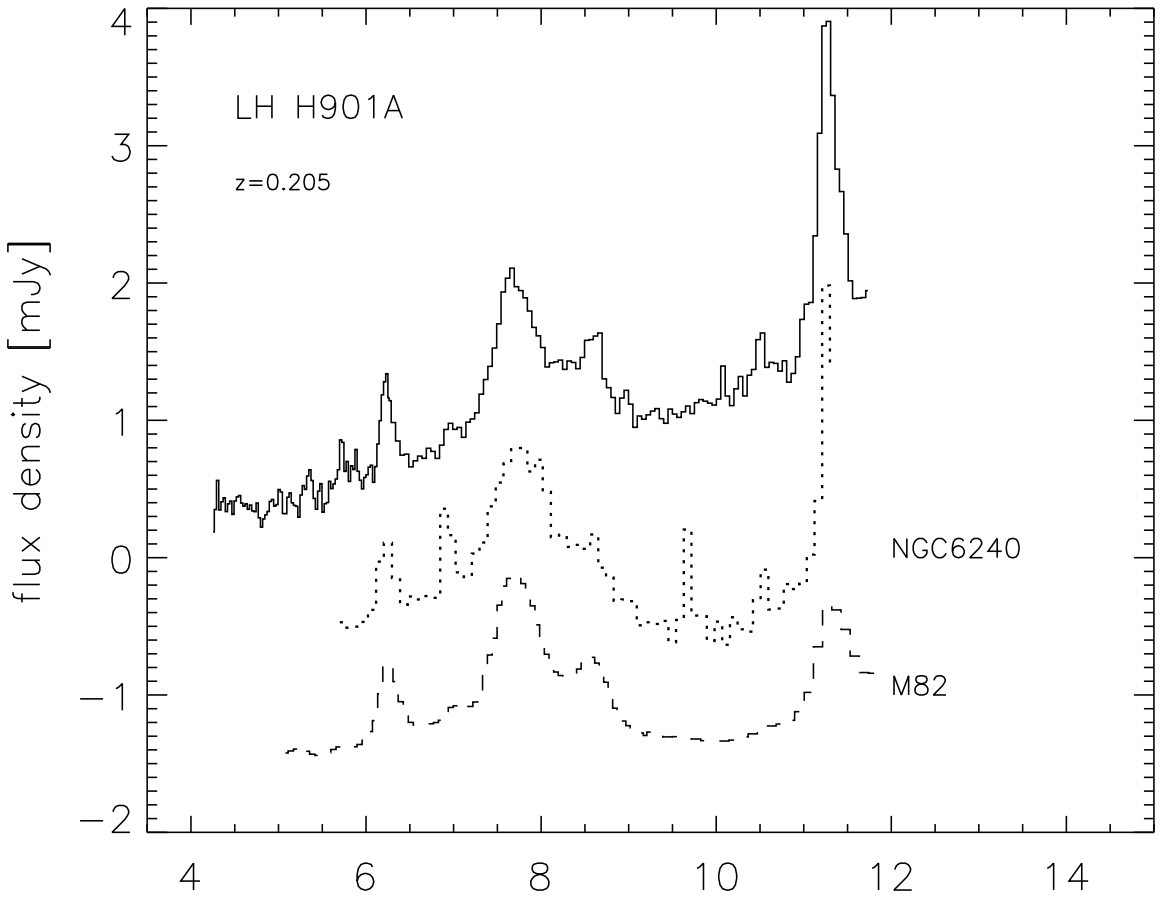

Fig. 2.— IRS spectrum of LH 901A. The dotted and dashed lines are the ISOPHOT-S spectrum of NGC 6240 (Lutz et al. 2003) and the ISOCAM-CVF spectrum of M 82 (Förster Schreiber et al. 2003), arbitrarily scaled.

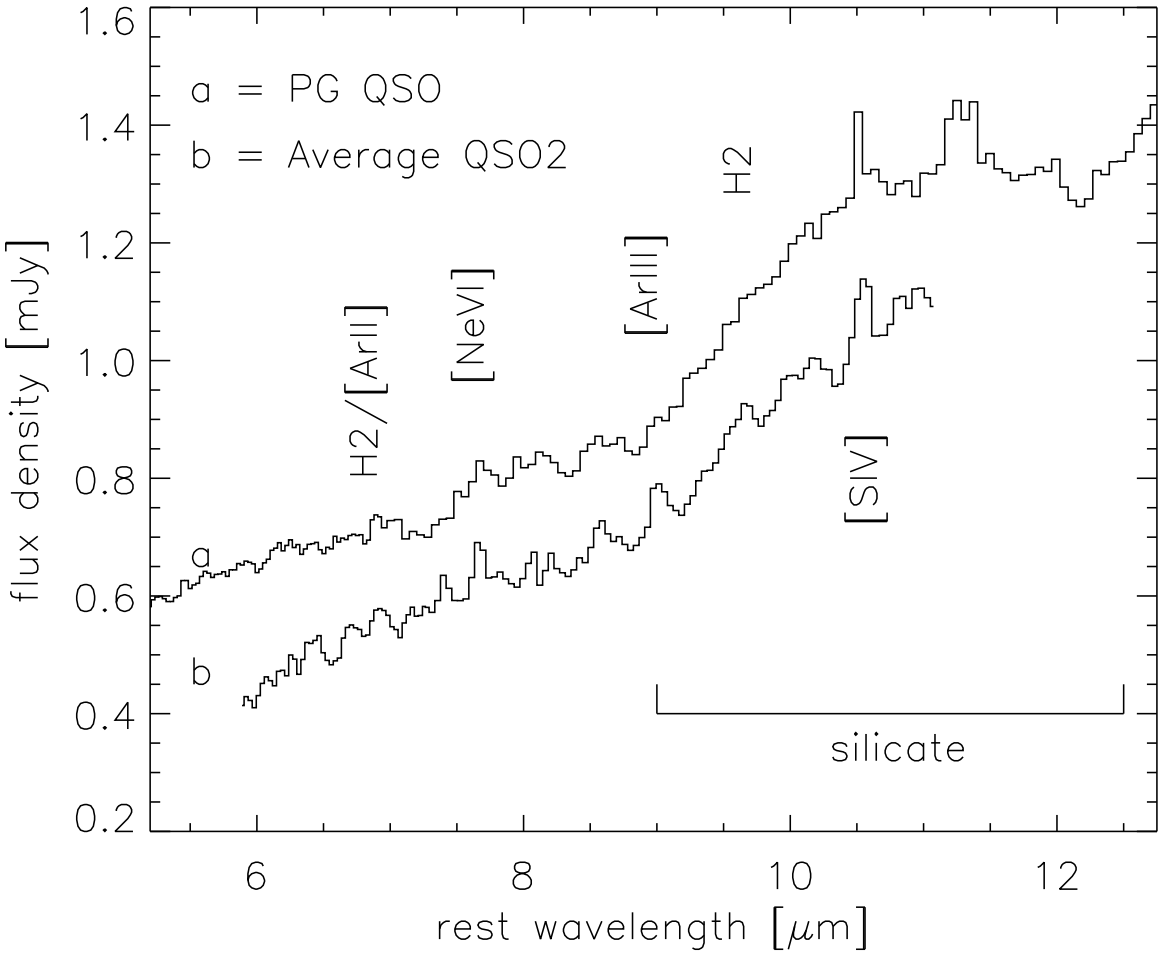

Fig. 3.— *a (top):* a typical PG QSO (PG1426+015, arbitrarily scaled), *b (bottom):* the average QSO2 spectrum.

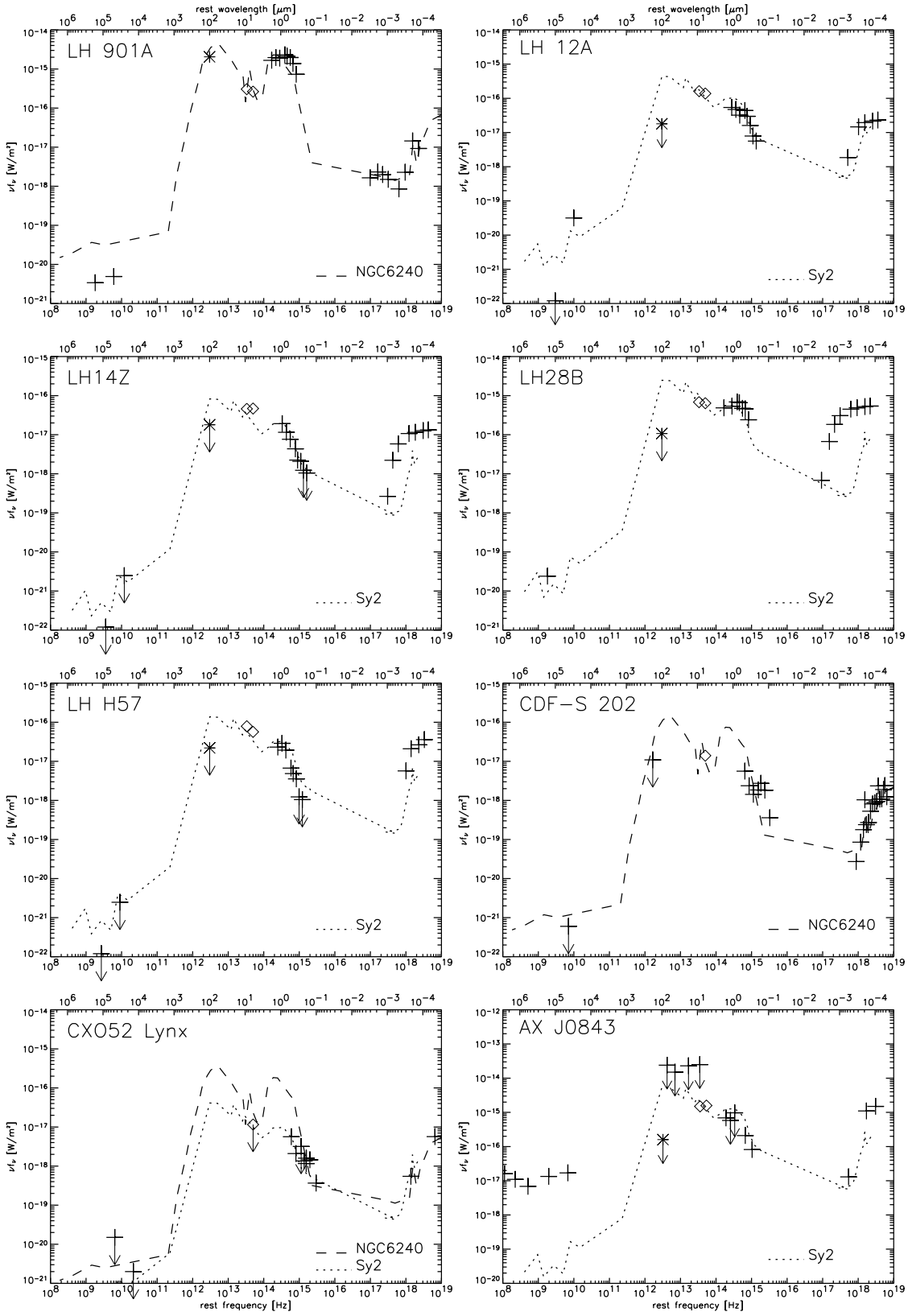

Fig. 4.— SEDs of the QSO2s. Diamonds represent our IRS spectra at 6 and 9 μm rest wavelength. *Dashed*: NGC 6240, *dotted*: average Sy2, scaled to the X-ray or near-IR. Asterisks at the SED peak are predictions from the PAH strength (see text).